

Textures and compressive properties of ferromagnetic shape-memory alloy $\text{Ni}_{48}\text{Mn}_{25}\text{Ga}_{22}\text{Co}_5$ prepared by isothermal forging process

Y.D. Wang^{a)} and D.Y. Cong

School of Materials and Metallurgy, Northeastern University, Shenyang 110004, People's Republic of China

R. Lin Peng

The Studsvik Neutron Research Laboratory (NFL), Uppsala University, S-61182 Nyköping, Sweden; and Department of Mechanical Engineering, Linköping University, S-58183 Linköping, Sweden

P. Zetterström

The Studsvik Neutron Research Laboratory (NFL), Uppsala University, S-61182 Nyköping, Sweden

Z.F. Zhang

Shenyang National Laboratory for Materials Science, Institute of Metal Research, Chinese Academy of Sciences, Shenyang 110016, People's Republic of China

X. Zhao and L. Zuo

School of Materials and Metallurgy, Northeastern University, Shenyang 110004, People's Republic of China

(Received 24 June 2005; accepted 30 November 2005)

A ferromagnetic shape-memory alloy $\text{Ni}_{48}\text{Mn}_{25}\text{Ga}_{22}\text{Co}_5$ was prepared by the induction melting and isothermal forging process. Dynamic recrystallization occurs during the isothermal forging. The deformation texture was studied by the neutron diffraction technique. The main texture components consist of (110)[$\bar{1}\bar{1}2$] and (001)[100], which suggested that in-plane plastic flow anisotropy should be expected in the as-forged condition. The uniaxial compression fracture strain in the forged alloy reaches over 9.5%. The final room-temperature fracture of the polycrystalline $\text{Ni}_{48}\text{Mn}_{25}\text{Ga}_{22}\text{Co}_5$ is controlled mainly by intergranular mode.

I. INTRODUCTION

Ferromagnetic shape-memory alloys (FSMAs) with chemical composition close to stoichiometric Ni_2MnGa have attracted much attention during the past few years due to the giant shape memory effect (SME) induced by magnetic fields.^{1,2} Intensive investigations on this alloy system have already been made regarding many scientific aspects, including crystal structure,^{3,4} magnetic properties,⁵ and responses of induced strain to magnetic fields.^{1,2} The large SME is attributed to the motion of twin boundaries or reselections of martensitic variants under applied magnetic fields. It is well known that the transformation strain and magnetic-field-induced strain are strongly dependent on the orientation of parent austenite and martensitic variants. Thus, explorations on some novel fabrication processes for enhancing preferred grain orientation (crystallographic texture) in the polycrystalline FSMAs do benefit the improvement of their

performance properties. The textured polycrystalline FSMAs can be obtained by using directional solidification, the rapid solidification technique, or plastic deformations. Recent investigations⁶ show that in spite of the very low ductility at room temperature and the poor formability at elevated temperature, the hot deformation process, a standard procedure used in the fabrications of some structural intermetallic alloys, was successful for preparations of polycrystalline NiMnGa alloys with the modification of microstructures. However, the development of textures has not been studied so far, partly due to the difficulty of measuring the textures in hot deformed coarse-grained NiMnGa alloys by the traditional x-ray diffraction method. Because of the high penetration of neutron beam and the large difference in the neutron scattering factors for Ni, Mn, and Ga atoms, the neutron diffraction technique becomes an ideal tool for characterizing the development of textures in this alloy system.

Considering practical applications as sensors and actuators, it is very important that the FSMAs should have higher martensitic transformation temperature (T_M) and Curie temperature (T_C). It has been found that T_M of

^{a)}Address all correspondence to this author.

e-mail: ydwang@mail.neu.edu.cn

DOI: 10.1557/JMR.2006.0079

Ni–Mn–Ga alloys is very sensitive to their composition,^{7,8} and some high-temperature Ni–Mn–Ga alloys with T_M higher than T_C have been achieved.^{9,10} However, T_C in Ni–Mn–Ga alloys does not strongly depend on the composition and has a value of around 370 K for a wide range of compositions close to Ni_2MnGa .^{9,10} Cherechukin et al.¹¹ found that a small amount of substitution of Co for Ni in Ni–Mn–Ga alloys increases T_C and decreases T_M slightly. Thus substitution of Co for Ni in the high-temperature Ni–Mn–Ga alloys can produce ferromagnetic Ni–Mn–Ga–Co alloys with high T_C close to T_M , by which a coupled magnetostructural transition may be realized and show great attractions in the development of alloy systems.^{5,12} On the other hand, the addition of Co allows for enhancement of the alloy ductility without changing crystal structure and overcomes the well-known brittleness in Ni–Mn–Ga alloys, which seriously hinders their practical application. Therefore, it is of both vital fundamental importance and practical interest to investigate the crystal structures, crystallographic textures, and mechanical behaviors in the Ni–Mn–Ga–Co alloy system. In the present paper, a $\text{Ni}_{48}\text{Mn}_{25}\text{Ga}_{22}\text{Co}_5$ alloy was prepared by induction melting and the isothermal forging process. The hot deformation textures of this alloy are characterized for the first time by the neutron diffraction technique and the mechanical behaviors of the forged alloy are reported. The possible mechanisms for the development of texture in the hot-forged alloy are discussed.

II. EXPERIMENTAL

A 380-g button ingot of $\text{Ni}_{48}\text{Mn}_{25}\text{Ga}_{22}\text{Co}_5$ (at.%), in the shape of paraboloid with a diameter of 55 mm at the bottom and a height of 36 mm, was prepared by repeated melting of the high purity constituent elements Ni, Mn, Ga, and Co in an induction furnace protected under argon atmosphere. The received ingot was sealed into a vacuum quartz tube and annealed at 900 °C for 52 h to create homogeneous microstructures. A thin layer of yttria was wiped on the surface of the annealed ingot to prevent oxidation during the subsequent hot forging. The annealed ingot was then sealed into a stainless steel jacket with an inner diameter of 55 mm, an outer diameter of 65 mm, and a height of 36 mm. The fiberglass was filled into the empty sections of the stainless steel jacket. The sealed ingot was heated to 950 °C and kept for 2 h, and then forged at 900 °C in the dies of cast Ni_3Al alloy under a strain rate of about 10^{-2} s^{-1} to a final strain of about 60%. Some powders were prepared from the as-forged sample for determining the crystal structure and phase-transformation temperatures. A cylindrical sample with the size of $16 \times \phi 5$ mm was cut by electro-discharge machine from the forged ingot, with the axial direction parallel to the uniaxial compression direction of the

thermal forging, for the texture measurements. A sample with the size of $4 \times 4 \times 8$ mm (with 8 mm along uniaxial compression direction of the thermal forging ingot) was also cut from the forged ingot for the compression experiment at room temperature, and the sample was compressed along the maximum length direction.

The phase-transformation temperatures were determined by a differential scanning calorimetry (DSC) measurement, with a heating and cooling rate of 10 °C/min. The neutron powder diffraction experiments were performed on beam line disordered materials structure measurement (SLAD) with the wavelength of 1.116 Å¹³ and pole figure measurements were taken on beam line residual stress and texture (REST) with the wavelength of 1.7 Å using the Eulerian cradle geometry, at the Studsvik Neutron Research Laboratory, Nyköping Sweden. The inverse pole figures were determined by the popLA software¹⁴ from three measured pole figures, i.e., (110), (112), and (312). The room-temperature compression experiment was carried out with a strain rate of 10^{-4} s^{-1} for measuring the stress versus strain curve of the forged alloy.

III. RESULTS AND DISCUSSION

The plastic flow is homogeneous on the macroscopic scale after hot forging and no micro-cracks were observed in the central part, in spite of some small cracks on the edge of the forged ingot. The microstructure of the hot-forged alloy is given in Fig. 1(a), showing some equiaxed grains with the size of 300–500 μm in diameter. The presence of martensitic twins can be clearly seen in the coarse-grained regime. Aside from those, some small grains with the size of 20–50 μm in diameter are also found in the grain boundaries of those coarse grains. The appearance of those small grains is obviously caused by the dynamic recrystallization during hot deformation, which has never been reported before. It should be noted that our hot deformation temperature is about 100 °C lower than that used by Besseghimi et al.⁶ A possible reason is that the dynamic recrystallization during hot deformation is promoted by the addition of Co in the Ni–Mn–Ga alloy system.

The DSC curve shown in Fig. 1(b) demonstrates that the martensitic transformation starting temperature M_s and finishing temperature M_f are 114 and 93 °C, respectively, and the austenitic transformation starting temperature A_s and finishing temperature A_f are 126 and 147 °C, respectively. The appearance of some split peaks during heating in the DSC curve is due to the existence of microstresses in the powders rather than the heterogeneity of chemical composition in the forged sample, as no split exothermic peaks appear in the cooling curve.

Figure 2 illustrates the neutron powder diffraction pattern of $\text{Ni}_{48}\text{Mn}_{25}\text{Ga}_{22}\text{Co}_5$ taken at room temperature,

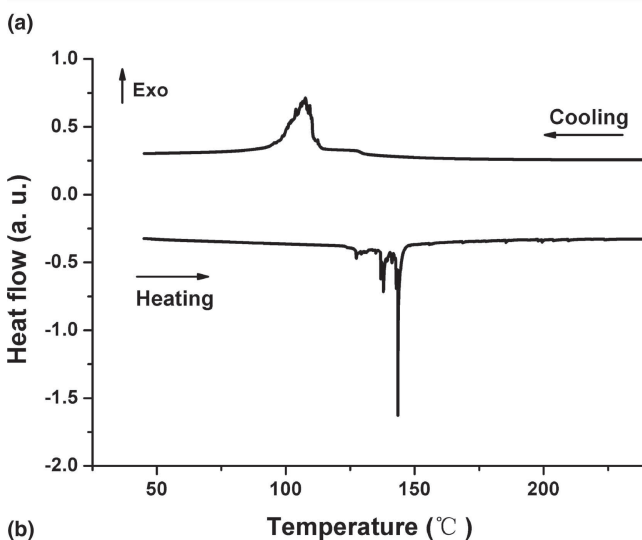
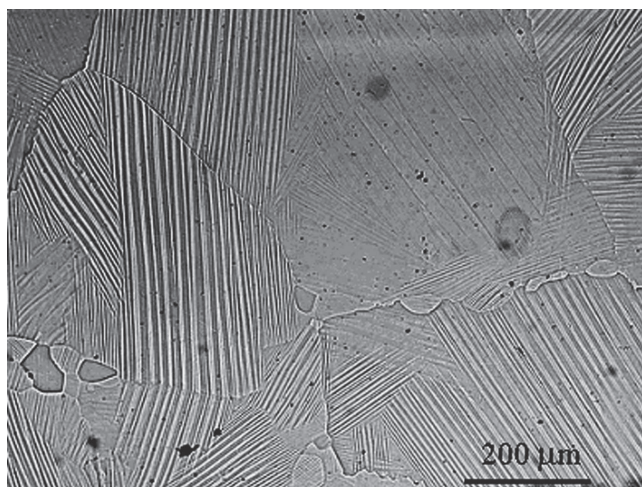


FIG. 1. (a) Microstructures after isothermal forging, and (b) DSC curve of the investigated alloy with a heating and cooling rate of $10\text{ }^\circ\text{C}/\text{min}$.

showing that the alloy has a single martensitic phase. All the intensity peaks in the pattern can be indexed well according to a tetragonal structure with $a = 3.888\text{ \AA}$ and $c = 6.484\text{ \AA}$, respectively. The space group of the structure is $I4/mmm$ (No. 139), which is in good agreement with that of ternary Ni–Mn–Ga alloys.^{3,15} The c/a ratio for the investigated alloy is 1.67, which is smaller than that found in $\text{Ni}_{53}\text{Mn}_{25}\text{Ga}_{22}$ ($a = 3.865\text{ \AA}$, $c = 6.596\text{ \AA}$, and $c/a = 1.71$).¹⁵ Thus it is inferred from the above neutron powder diffraction analysis that the addition of Co up to 5 at.% to Ni–Mn–Ga alloy does not alter its crystal structure, but the c/a ratio is dramatically reduced. It should be noted that several previous investigations^{1–3,5,9} on the crystal structure of Ni–Mn–Ga alloy system by x-ray diffraction technique cannot give full information on crystal structure due to the similar x-ray scattering factors for Ni, Mn, and Ga atoms. Rietveld refinement on the occupation of Co in this alloy from neutron powder diffraction data is now in progress.

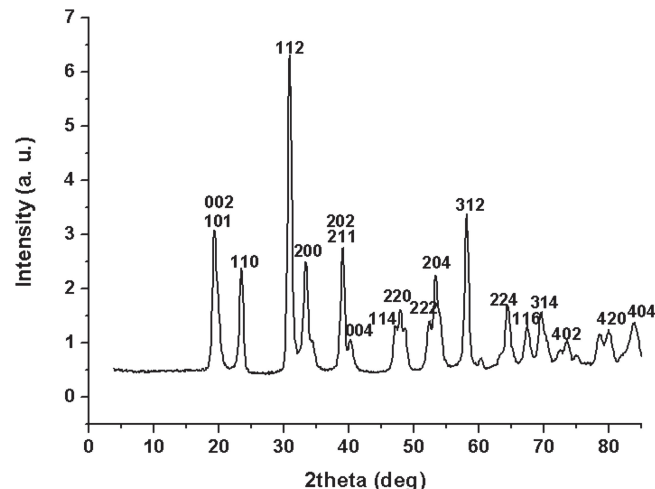


FIG. 2. Powder neutron diffraction profile of the $\text{Ni}_{48}\text{Mn}_{25}\text{Ga}_{22}\text{Co}_5$ alloy measured at room temperature. The miller index is marked as $I4/mmm$ space group (No. 139).

The texture of the hot-forged $\text{Ni}_{48}\text{Mn}_{25}\text{Ga}_{22}\text{Co}_5$ alloy illustrated by the three measured (110)-, (112)-, and (312)-pole figures is shown in Fig. 3. It can be seen from these measured pole figures that some strong texture components developed in the stage of hot deformation. Aside from this, the lack of axial symmetry observed in those pole figures suggests that in-plane plastic flow anisotropy should be expected in this material in the as-forged condition. Further deformation would be required to obtain the expected uniaxial textures.

The inverse pole figures for the compression axis (CA) and the radial direction (RD) of the as-forged sample are shown in Fig. 4. It can be seen from the inverse pole figures that the main texture components in the as-forged sample consist of (110)[$\bar{1}\bar{1}2$] (brass type) and (001)[100] (cube). Here, we use a texture representation of $(hkl)[uvw]$ with a notation of the (hkl) plane perpendicular to the CA and the $[uvw]$ direction [the normal direction of (uvw) plane] parallel to the RD of the forged ingot. The brass-type texture can be also seen from the distributions of $\{1\bar{1}2\}$ -poles and the strong maxima along RD indicated in the $\{112\}$ -pole figure as shown in Fig. 3(b). In addition, unmistakable signs of a $\langle 100 \rangle$ fiber can be clearly seen from the $\{110\}$ -pole figure illustrated in Fig. 3(a). The anisotropic textures in the forging plane may be inherited from the initial structure after casting.

The texture analysis mentioned above is based only on the measurements at room temperature in martensitic phase, not in the high-temperature parent phase that was actually deformed. Then the issue of transformation textures, studied extensively in steels,^{16,17} titanium alloys,¹⁸ Cu–Zn alloys,^{19,20} NiTi shape-memory alloys,²¹ and so on, may arise. Although the deformation mechanisms for both the parent phase with a cubic structure and the martensitic phase with a body centered tetragonal structure in

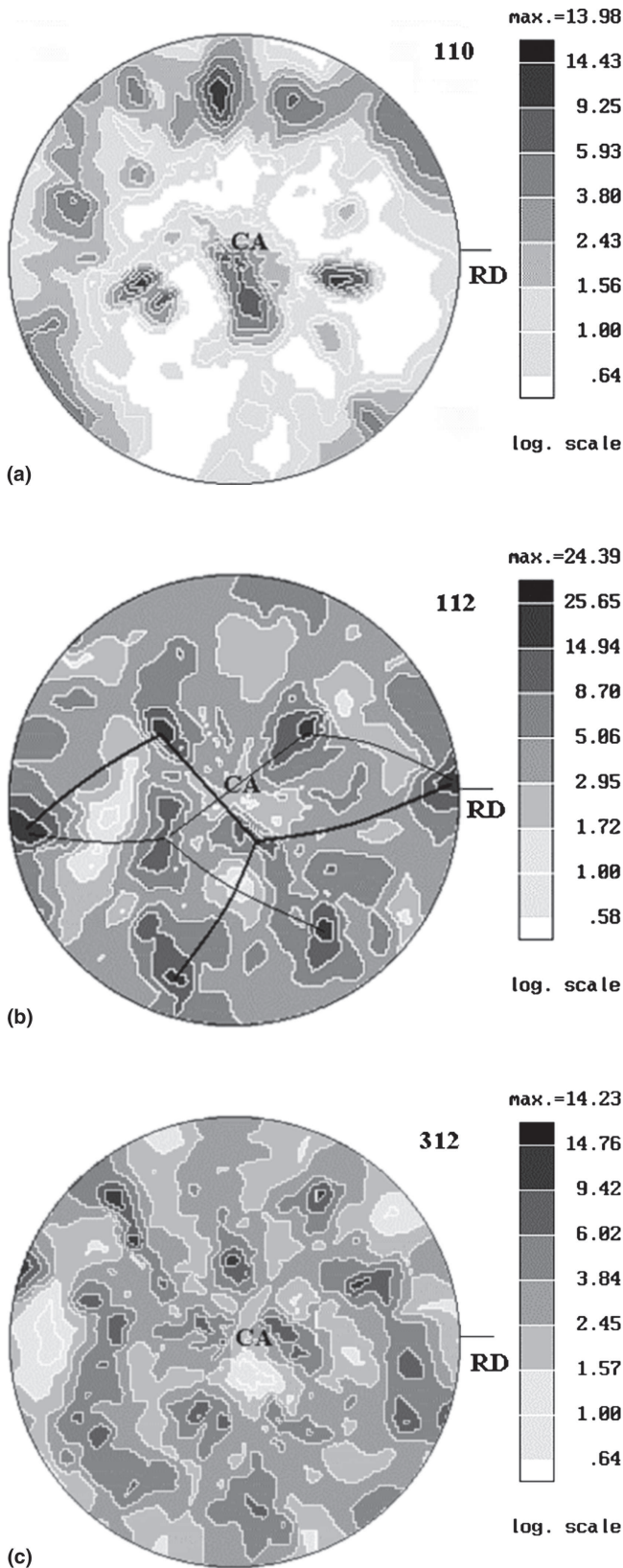


FIG. 3. Measured (a) (110), (b) (112), and (c) (312) pole figures of texture in the hot-forged $\text{Ni}_{48}\text{Mn}_{25}\text{Ga}_{22}\text{Co}_5$. CA, compression axis; RD, radial direction.

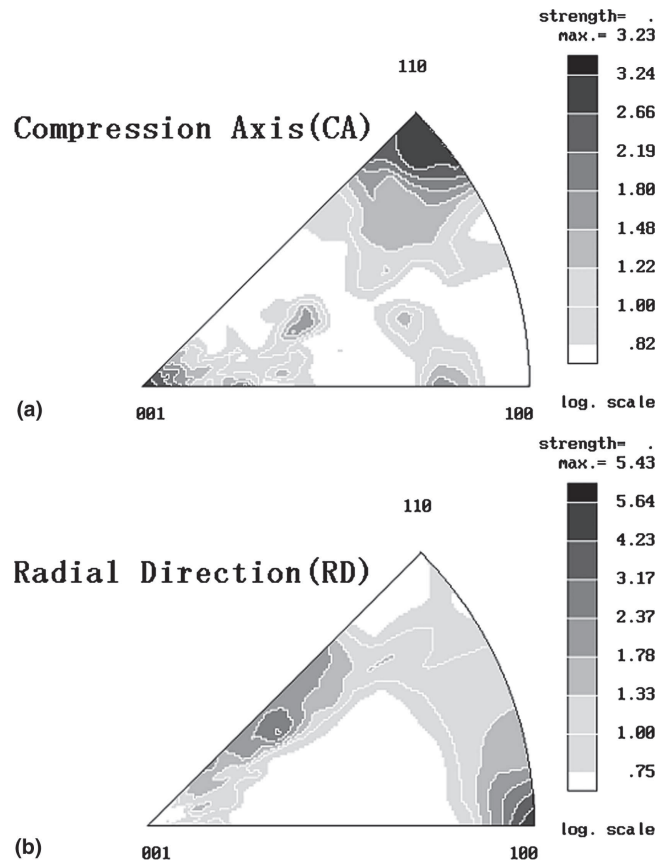


FIG. 4. Inverse pole figures of (a) compression axis (CA) and (b) radial direction (RD) in the hot-forged $\text{Ni}_{48}\text{Mn}_{25}\text{Ga}_{22}\text{Co}_5$. The inverse pole figures are calculated from the measured pole figures by the popLA software.¹⁴

Ni–Mn–Ga alloy system are not clear so far, we may make a predictive analysis of the texture inheritance using the valuable texture information obtained at room temperature. The parent phase in the Ni–Mn–Ga alloy system has been confirmed to be the cubic Heusler structure (space group $Fm\bar{3}m$, No. 225) by neutron diffraction experiments.^{4,22} Based on the previous publications,^{22,23} the martensitic transformation in this alloy system was described as a simple dilation along one of the $\langle 001 \rangle$ of the cubic parent phase to the $[001]$ of the martensitic phase, i.e., $(001)_P // (001)_M$, and a contraction along two $\langle 100 \rangle$ of the parent phase to the $[110]$ and $[1\bar{1}0]$ of the martensitic phase, i.e., $(100)_P // (110)_M$ and $(010)_P // (1\bar{1}0)_M$. Therefore, it can be deduced from the texture components $(110)[1\bar{1}2]$ and $(001)[100]$ in the martensitic phase that the main texture components in the parent phase are $(100)[0\bar{1}4]$ and $(001)[110]$. However, this prediction is only based on the ideal crystallographic orientation relationship between the parent phase and the martensitic phase, and the actual transformation textures may be different due to the influence of the variant selection and other complex factors during martensitic transformation. Deep understanding into the

transformation textures in this alloy system still needs further investigations with in situ texture measurements performed both in parent phase and martensitic phase, and/or related texture simulation techniques.

The compression stress versus strain curve of the $\text{Ni}_{48}\text{Mn}_{25}\text{Ga}_{22}\text{Co}_5$ alloy is shown in Fig. 5, from which it can be seen that there is a very high work hardening stage following the elastic deformation stage. The stress becomes maximum at around 9.5% and decreases by further loading indicating some cracks already appear. Figures 6(a)–6(c) exhibit the typical scanning electron microscopy (SEM) observations of the fracture characteristics of hot-forged alloy under uniaxial compressive loading. It can be seen from the observed fracture morphology that the intergranular fracture occurs under the compression mode in the hot-forged sample, and some shear bands with the mean spacing of about $20\ \mu\text{m}$ are well developed in some regions. Those deformation bands are inclined to the stress axis under different angles varying from region to region, as marked in Fig. 6(a). It appears that the intergranular fracture initiates at those high-angle grain boundaries due to the large incompatibility of plastic deformation. Some cracks can also be observed inside some shear bands [Fig. 6(c)]. It implies that the nucleation and propagation of cracks dominates the fracture behavior of the hot-forged alloy.

The yield stress, maximum strength, and fracture strain under compression mode reach 205 MPa, 880 MPa, and 9.5%, respectively. The fracture strain under compression mode of the hot-forged $\text{Ni}_{48}\text{Mn}_{25}\text{Ga}_{22}\text{Co}_5$ is much higher than that found in Ni–Mn–Ga (2%) and Ni–Mn–Ga–Nd (6%) in the parent phase, as reported by Tsuchiya et al.²⁴ Although a maximum shape strain as high as 20% can be observed for the tetragonal martensite in the single crystal of Ni–Mn–Ga alloy,⁹ the fracture strain for polycrystalline Ni–Mn–Ga alloys is generally

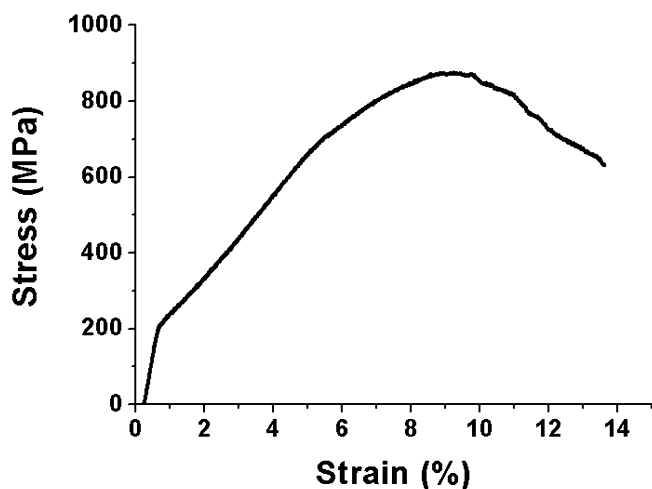
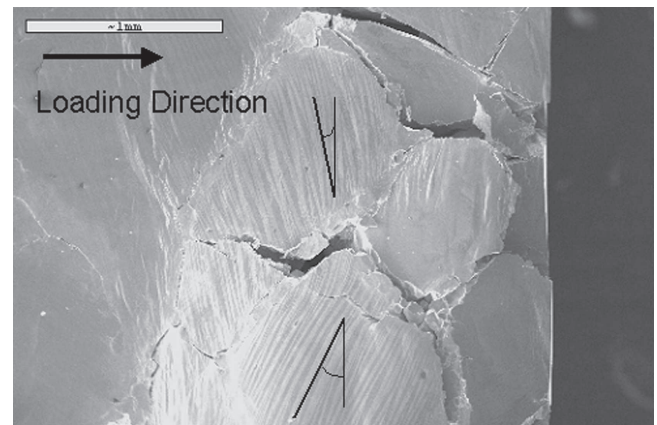
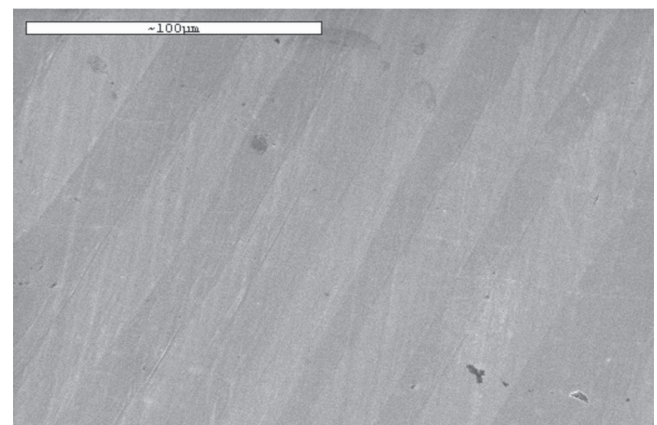


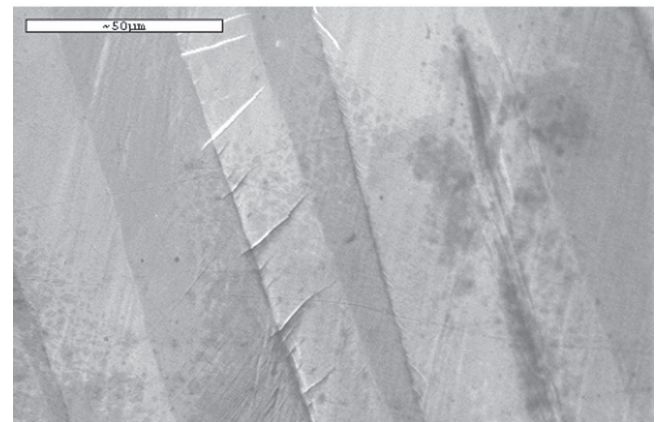
FIG. 5. Compressive stress versus strain curve of the hot-forged $\text{Ni}_{48}\text{Mn}_{25}\text{Ga}_{22}\text{Co}_5$.



(a)



(b)



(c)

FIG. 6. Compressive fracture morphology of the hot-forged $\text{Ni}_{48}\text{Mn}_{25}\text{Ga}_{22}\text{Co}_5$: (a) macro-appearance of the fractured sample, (b) shear bands, and (c) micro-cracks inside the shear bands. The loading direction is marked in (a).

still small. Actually, the fracture value in the hot-forged $\text{Ni}_{48}\text{Mn}_{25}\text{Ga}_{22}\text{Co}_5$ is comparable to that observed in the high-temperature shape-memory alloys NiAl (10%) and NiMn (11%).²⁵

The observed larger fracture strain can be partly explained by the variant reorientation (twinning/detwinning)

mechanism when the sample is deformed in the martensitic state, while some further mechanisms should also be considered. We have observed a dramatic change in texture after just 3.3% of plastic deformation at room temperature, and the new texture components disappear after annealing at 250 °C (above the austenitic transformation point). This indicates that the twinning/detwinning indeed plays a role in the beginning of plastic deformation. However, the recovery strain is about 2.4% after annealing, which means that other mechanisms, such as dislocation slipping and/or grain boundary gliding, are also important for the plastic deformation at room temperature. The present authors believe that the larger compression fracture strain in the quaternary Ni₄₈Mn₂₅Ga₂₂Co₅ alloy is also attributed to the dynamic recrystallization observed in the isothermal forging process. Further investigations are still required for better understanding of the mechanisms to control plastic behaviors in the present hot-forged alloy.

IV. CONCLUSIONS

In summary, we report the crystal structure, hot deformation textures, and mechanical properties in a ferromagnetic shape memory alloy Ni₄₈Mn₂₅Ga₂₂Co₅ prepared by induction melting and the hot forging process. The results show that the investigated alloy has a tetragonal, *I4/mmm* structure with a *c/a* ratio of 1.67 at room temperature. Dynamic recrystallization occurs during the hot forging. The results of the texture measurements show strong textures with the main texture components consisting of (110)[1 $\bar{1}$ 2] and (001)[100]. The lack of axial symmetry observed in the pole figures suggests that in-plane plastic flow anisotropy should be expected in the as-forged condition. The yield stress, maximum stress, and fracture strain of the hot-forged Ni₄₈Mn₂₅Ga₂₂Co₅ are 205 MPa, 880 MPa, and 9.5%, respectively. Intergranular fracture occurs and some shear bands with the mean spacing of about 20 μ m are developed under the compression mode in the present hot-forged alloy.

ACKNOWLEDGMENTS

The authors are grateful to the National Natural Science Foundation of China (Grant Nos. 50531020 and 50471026), the Ministry of Education of China (with the New-Century Excellent Students Fund NCET-04-0282), and the Swedish Research Council in the frame of SIDA project (Grant No. 348-2004-3475) for their financial support.

REFERENCES

1. A. Sozinov, A.A. Likhachev, N. Lanska, and K. Ullakko: Giant magnetic-field-induced strain in NiMnGa seven-layered martensitic phase. *Appl. Phys. Lett.* **80**, 1746 (2002).
2. S.J. Murray, M.A. Marioni, A.M. Kukla, J. Robinson, R.C. O'Handley, and S.M. Allen: Large field induced strain in single crystalline Ni-Mn-Ga ferromagnetic shape memory alloy. *J. Appl. Phys.* **87**, 5774 (2000).
3. B. Wedel, M. Suzuki, Y. Murakami, C. Wedel, T. Suzuki, D. Shindo, and K. Itagaki: Low temperature crystal structure of Ni-Mn-Ga alloys. *J. Alloys Compd.* **290**, 137 (1999).
4. P.J. Webster, K.R.A. Ziebeck, S.L. Town, and M.S. Peak: Magnetic order and Phase transformation in Ni₂MnGa. *Philos. Mag. B* **49**, 295 (1984).
5. V.V. Khovailo, T. Takagi, J. Tani, R.Z. Levitin, A.A. Cherechukin, M. Matsumoto, and R. Note: Magnetic properties of Ni_{2.18}Mn_{0.82}Ga Heusler alloys with a coupled magnetostructural transition. *Phys. Rev. B* **65**, 092410 (2002).
6. S. Besseghimi, E. Villa, F. Passaretti, M. Pini, and F. Bonfanti: Plastic deformation of NiMnGa polycrystals. *Mater. Sci. Eng. A* **378**, 415 (2004).
7. N. Lanska, O. Söderberg, A. Sozinov, Y. Ge, K. Ullakko, and V.K. Lindroos: Composition and temperature dependence of the crystal structure of Ni-Mn-Ga alloys. *J. Appl. Phys.* **95**, 8074 (2004).
8. V.A. Chernenko, E. Cesari, V.V. Kokorin, and I.N. Vitenko: The development of new ferromagnetic shape memory alloys in Ni-Mn-Ga system. *Scripta Metall. Mater.* **33**, 1239 (1995).
9. H. Xu, Y. Ma, and C. Jiang: A high-temperature shape-memory alloy Ni₅₄Mn₂₅Ga₂₁. *Appl. Phys. Lett.* **82**, 3206 (2003).
10. V.A. Chernenko, V. L'Vov, J. Pons, and E. Cesari: Superelasticity in high-temperature Ni-Mn-Ga alloys. *J. Appl. Phys.* **93**, 2394 (2003).
11. A.A. Cherechukin, T. Takagi, H. Miki, M. Matsumoto, and M. Ohtsuka: Influence of three-dimensional transition elements on magnetic and structural phase transitions of Ni-Mn-Ga alloys. *J. Appl. Phys.* **95**, 1740 (2004).
12. C. Jiang, G. Feng, and H. Xu: Co-occurrence of magnetic and structural transitions in the Heusler alloy Ni₅₃Mn₂₅Ga₂₂. *Appl. Phys. Lett.* **80**, 1619 (2002).
13. A. Wannberg, A. Mellergård, P. Zetterström, R. Delaplane, M. Grönros, L-E. Karlsson, and R.L. McGreevy: SLAD: A neutron diffractometer for the study of disordered materials. *J. Neutron Res.* **8**, 133 (1999).
14. U.F. Kocks, J.S. Kallend, H.R. Wenk, A.D. Rollett, and S.I. Wright: *PopLA: Preferred Orientation Package—Los Alamos* (Los Alamos National Laboratory, Los Alamos, NM, 1995).
15. D.Y. Cong, P. Zetterström, Y.D. Wang, R. Delaplane, R. Lin Peng, X. Zhao, and L. Zuo: Crystal structure and phase transformation in Ni₅₃Mn₂₅Ga₂₂ shape memory alloy from 20 K to 473 K. *Appl. Phys. Lett.* **87**, 111906 (2005).
16. R.K. Ray, J.J. Jonas, M.P. Butrón-Guillén, and J. Savoie: Transformation textures in steels. *ISIJ Int.* **34**, 927 (1994).
17. G. Brückner and G. Gottstein: Transformation textures during diffusional $\alpha \rightarrow \gamma \rightarrow \alpha$ phase transformations in ferritic steels. *ISIJ Int.* **41**, 468 (2001).
18. S.V. Divinski, V.N. Dnieprenko, and O.M. Ivasishin: Effect of phase transformation on texture formation in Ti-base alloys. *Mater. Sci. Eng. A* **243**, 201 (1998).
19. T. Sakata, H.Y. Yasuda, and Y. Umakoshi: Formation process of transformation texture from the β to α phase in Cu-42 mass% Zn alloy. *Scripta Mater.* **43**, 411 (2000).
20. H.Y. Yasuda, T. Sakata, and Y. Umakoshi: Variant selection in transformation texture from the β to α phase in Cu-40 mass% Zn alloy. *Acta Mater.* **47**, 1923 (1999).

21. H. Inoue, M. Ishio, and T. Takasugi: Texture of TiNi shape memory alloy sheets produced by roll-bonding and solid phase reaction from elementary metals. *Acta Mater.* **51**, 6373 (2003).
22. P.J. Brown, J. Crangle, T. Kanomata, M. Matsumoto, K-U. Neumann, B. Ouladdiaf, and K.R.A. Ziebeck: The crystal structure and phase transitions of the magnetic shape memory compound Ni_2MnGa . *J. Phys.: Condens. Matter* **14**, 10159 (2002).
23. J. Pons, V.A. Chernenko, R. Santamarta, and E. Cesari: Crystal structures of martensitic phases in Ni–Mn–Ga shape memory alloys. *Acta Mater.* **48**, 3027 (2000).
24. K. Tsuchiya, A. Tsutsumi, H. Ohtsuka, and M. Umemoto: Modification of Ni–Mn–Ga ferromagnetic shape memory alloy by addition of rare earth elements. *Mater. Sci. Eng. A* **378**, 370 (2004).
25. K.K. Jee, P.L. Potapov, S.Y. Song, and M.C. Shin: Shape memory effect in NiAl and NiMn-based alloys. *Scripta Mater.* **36**, 207 (1997).